Chalcogenide Letters Vol. 18, No. 10, October 2021, p. 649 - 665

Comparative analysis of the effect of annealing temperature on the structural and optical properties of chemically deposited CeO_2/ZnO and CeO_2/NiO core-shell thin films for photovoltaic and optoelectronic applications

P. N. Kalu[a], C. Augustine[a,*], A. N. Nwachukwu[a], R. A. Chikwenze[a], S. O. Amadi[a], B. J. Robert[b], P.E. Okpani[c], T. O. Daniel[a] , C. N. Ukwu[a], E. P. Obot[a], C. O. Dike[a], R.O. Okoro[d]

[a]*Department of Physics, Alex Ekwueme Federal University Ndufu-Alike, Ikwo, Ebonyi State, Nigeria*

[b]*Department of Electrical/Electronics Engineering Technology, Akanu Ibiam Federal Polytechnic, Unwana, Ebonyi State, Nigeria*

[c]*Department of Electrical and Electronic Engineering,, Alex Ekwueme Federal University Ndufu-Alike, Ikwo, Ebonyi State, Nigeria*

[d]*Department of Physics, Ebonyi State College of Education, Ikwo, Ebonyi State, Nigeria*

This paper describes the deposition and characterization of CeO_2/ZnO and CeO_2/NiO core-shell thin films with emphasis on the effect of post deposition temperature on the optical properties and structural patterns. The structural temperature-dependent analysis indicated different XRD patterns for both films. However, both films are polycrystalline as depicted by the various peaks in the XRD diffractograms. The SEM images for both films differ in terms of their particle aggregation and distribution. The dependence of the transmittance, absorption coefficient, band gap, refractive index, extinction coefficient, imaginary dielectric constant on annealing temperature were investigated. The results showed that the transmittances of the films were significantly reduced by the heat treatments. The transmittance reduced from 92% to 65% for CeO_2/ZnO film samples and 63% to 30% for CeO_2/NiO film samples. The band gap showed considerable variation with annealing temperatures. The band gaps of all samples were in ranges of 1.75–3.85 eV and 3.50-3.88eV for CeO_2/ZnO and CeO_2/NiO core-shell thin films respectively. The values of the energy band gap strongly indicate that the films can be used in different optoelectronic applications including solar photovoltaic.

(Received June, 21, 2021; Accepted October 21, 2021)

Keywords: Band gap, Temperature, Thin film, Transmittance, Characterization

1. Introduction

The present growing interest in photovoltaic conversion is a consequence of the concern to identify future sources of energy that will be inexpensive as well as consistent with the maintenance and safety of the environment [1]. Conversion of solar energy to useable photovoltaic energy is believed to be among the most promising techniques of overcoming present and future increasing energy demands when conventional sources of energy are being run short [1]. In terms of human history, the life of the sun is effectively infinite, its energy is radiated to the earth whether it is directly used or not, and the use of photovoltaic for direct conversion of solar energy introduces no direct contamination of the environment [1]. Solar thermal and photovoltaic technologies are expected to be quite relevant in Nigeria. Presently, only minimal amount of solar energy is being utilized but the future sees vast application in this area. The photovoltaic application is particularly suited for remote areas because in remote and far flung areas, the cost of installation of grid stations more than overweighs their advantages and the electricity becomes very expensive. Although the advantages of solar energy conversion to electricity through solar

* Corresponding authors: emmyaustine2003@yahoo.com

https://doi.org/10.15251/CL.2021.1810.649

cells are huge, its wide use has been hindered by high cost of silicon based solar cell which presently predominates the photovoltaic industry [1].

The need for alternative materials with low production cost that can serve as substitutes for crystalline silicon solar cells cannot be over-emphasized. Recently, thin film solar cell is currently gaining recognition due to its low cost in comparison to the high cost of silicon based solar cell which has made the entire production of solar energy to be expensive [2]. Thin film approach of producing solar cells reduces cost by using small amount of material and inexpensive processing. Thin film solar cells represent one such technology which is now being actively pursued using many different material systems. Thin film polycrystalline solar cells require less material and are more suited to mass- production techniques and are therefore viewed as a viable low-cost option.

An essential parameter for thin film solar cell is the band gap. Wide-band gap (WBG) materials have band gaps on the order of 2 to 4eV [3, 4]. They permits devices to operate at much higher voltages, frequencies and temperatures than convectional semiconductor materials. Cerium oxide (CeO) is an important wide band gap material of about 3.2eV and transparent in the visible region (400-800nm) [5, 6]. Zinc oxide (ZnO) thin film is an important transparent conducting oxide with direct wide band gap of about 3.37eV at room temperature [7]. Because of its wide band gap, ZnO thin film can be use as window layer in solar cell fabrication [8]. Nickel oxide (NiO) thin films is a transition metal oxide with excellent chemical and thermal stability [9, 10]. It has potential applications in such areas as electro-chromic display devices, anti-ferromagnetic layers, solar thermal absorber and as cathode material for alkaline batteries [11-13]. Some other interesting electronic properties of NiO thin film include its wide band gap range of 3.6-4.0eV [14]. Combining these oxides to form a core-shell can alter the band gap for special applications.

Presently, there are myriads of research works on the synthesis of advanced core/shell heterostructures with fascinating synergetic properties or multifunctionalities offered by the composite nanostructures. The heterostructured architecture can exhibit enhanced properties through reinforcement or modification of each other. Many core/shell heterostructures such as TiO_2/CuO [15], PbS/NiO [16], CuO/PbS [17], Mn_3O_4/PbS [18], PbS/CdO [19] and PbS/NiO/CdO [20] have been explored, and enhanced properties have been demonstrated. In this paper, we report on the deposition of CeO/ZnO and CeO/NiO core-shell thin films using chemical bath deposition technique, with emphasis on the effect of post deposition temperature on the structural and optical properties.

2. Experimental

The chemicals used for the deposition of CeO/ZnO and CeO/NiO thin films include Zinc Sulphate ($ZnSO_4$), Nickel Sulphate ($NiSO_4$), Cerium Nitrate [$Ce(NO_3)_2$], and Ammonia (NH_3) analytical grade. Routine laboratory equipment such as beakers, reagent bottles, measuring cylinders, syringes, thermometer, magnetic stirrer, P^H meter, conical flasks and electric oven, were employed for the film deposition. The microscopic glass slides used as substrates prior to deposition were soaked in concentrated hydrochloric acid for 24 hours, removed and washed with foam-sponge in ethanol and finally rinsed in distilled water. Thereafter, they were then drip dried in air. The degreased, cleaned surface has the advantage of providing nucleation centers for the growth of the films, hence, yielding highly adhesive and uniformly deposited films. The solution growth of the thin films involved measuring with syringes desired volumes of definite molar solutions of the required chemicals for a particular precursor compound specified in the relevant sections into growth baths (50-100ml beakers) to form the growth mixture. The growth mixtures were topped with specific volume of distilled water and stirred with magnetic stirrer. Pre-cleaned glass substrates were then inserted vertically into the growth mixtures using synthetic foam. Synthetic rubber foam was used as cover to the reaction bath to protect it from dust particles and other environmental impurities as well as to suspend the substrate into open bath. This arrangement did not allow for an airtight reaction bath. This will prevent condensation on the inner surface of the cover. The set-up were each placed in the chamber of an oven set at the desired constant temperatures for specified periods. Fig.1 depicts a typical experimental set-up for the

deposition thin film using chemical bath deposition method. Thermo scientific GENESYS 10S model UV-VIS spectrophotometer was used to carry out the transmittance measurements in the wavelength range of 300-1000 nm from which optical properties were estimated.

2.1. Deposition of the Core (C_eO) Thin Films

In order to deposit the core, 15ml of 0.2M $Ce(NO_3)_2$ and 15ml of 0.2M of sodium thiosulphate with 2 drops of NH_3 (ammonia) were mixed in a chemical bath. The bath was allowed to stand for 1 hour at a temperature of 70^0C. The kinetics of the chemical reaction proceeded as follows;

$$Ce(NO_3)_2 \rightarrow Ce^{2+} + NO_3^{2-}$$
$$NH_3.H_2O \rightarrow NH_4^{+} + OH^{-}$$
$$Ce^{2+} + OH^{-} \rightarrow Ce(OH)_2$$
$$Ce(OH)_2 \rightarrow CeO + H_2O$$

2.2. Deposition of CeO/ZnO Core -Shell Thin Film

To deposit CeO_2/ZnO core-shell thin film, four glass slides of CeO deposits were inserted into a chemical bath containing 15mls of $ZnSO_4$, 5mls of ammonia solution and 15mls of water in that order. The chemical reaction for the formation of ZnO is given as:

$$ZnSO_4 \rightarrow Zn^{2+} + SO_4^{2-}$$
$$Zn^{2+} + OH^{-} \rightarrow Zn(OH)_2$$
$$Zn(OH)_2 \rightarrow ZnO + H_2O$$

2.3. CeO/NiO Core- Shell Thin Film

The deposition of CeO/NiO core-shell thin film was accomplished by inserting the glass slides made up of CeO deposits into a chemical bath containing 15m of $NiSO_4$, 5ml of NH_3 solution and 15ml of H_2O. The bath was maintained for 1hour at a temperature of 70^0C. The chemical reaction involved in the formation of NiO is as shown below;

$$Ni(SO_4)_2 \rightarrow Ni^{2+} + SO_4^{2-}$$
$$Ni^{2+} + 2(OH)^{-} \rightarrow Ni(OH)_2$$
$$Ni(OH)_2 \rightarrow NiO + H_2O$$

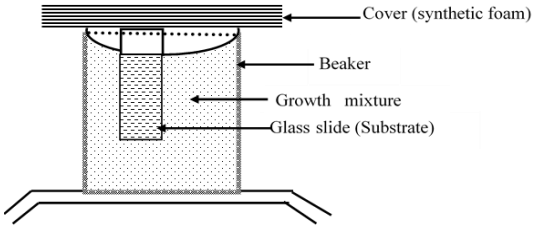

Fig. 1. Experimental set-up of solution growth deposition of thin films.

3. Results and Discussion

3.1. Energy Dispersive X-ray Fluorescence (EDXRF) Analysis

Figures 1 and 2 show the EDXRF analysis for CeO_2/ZnO and CeO_2/NiO core /shell thin films respectively. Fig.1 shows that cerium peak was recorded at 3.0keV, oxygen peak at 0.5keV and zinc peak at around 3.0KeV confirming the formation of CeO_2/ZnO thin film. Peak of silicon and sulphur were also noticed. From fig. 2, highest peak for cerium was recorded at 3.0keV, 1.0KeV for oxygen and 3.0KeV for nickel confirming the formation of CeO_2/NiO thin films. The peaks for other element could have come from glass and some impurities.

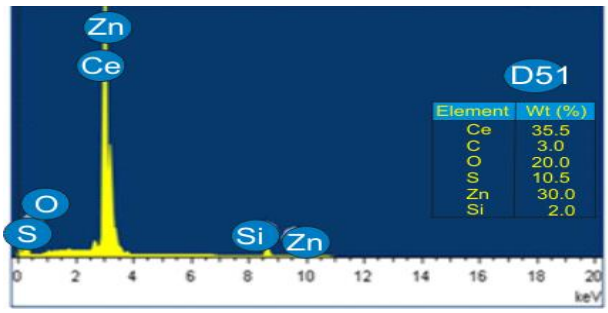

Fig. 1. EDXRF for CeO_2/ZnO core-shell thin film.

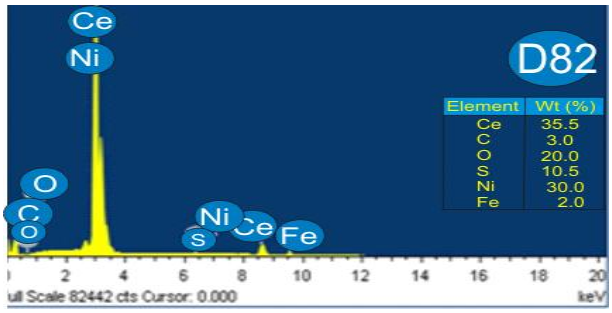

Fig. 2. EDXRF for CeO_2/NiO core-shell thin film.

3.2. Structural analysis

The XRD patterns of CeO_2/ZnO and CeO_2/NiO core /shell thin films are shown in figures 3, 4, 5 and 6 for as-deposited, annealed at 100^{o}C, 150^{o}C and 200^{o}C respectively. The multiple peaks exhibited by the films indicate their polycrystalline nature. In all the XRD patterns, CeO_2/ZnO films exhibited highest peak intensities compared to CeO_2/NiO films. For as-deposited samples, the peak intensity of CeO_2/ZnO films is about 8000 counts corresponding to 2θ angle of 10^{o}C while that of CeO_2/NiO films, is 2000 counts at angle of 10^{o}C. In the case of annealed at 100^{o}C, the peak intensities are (3000 counts, 5^{o}C) and (2000 counts, 30^{o}C) for CeO_2/ZnO and CeO_2/NiO core /shell thin films respectively. When annealing temperature increased to 150^{o}C, the peak intensities are (4800 counts, 10^{o}C) and (17500 counts, 10^{o}C) for CeO_2/ZnO and CeO_2/NiO films respectively. Further increasing the annealing temperature to 200^{o}C, the peak intensity for CeO_2/ZnO is about 10000 at 12.5^{o}C while that of CeO_2/NiO is about 2000 at 10^{o}C. The higher peak intensities exhibited by CeO_2/ZnO films is indication of better crystalinity compared to CeO_2/NiO films.

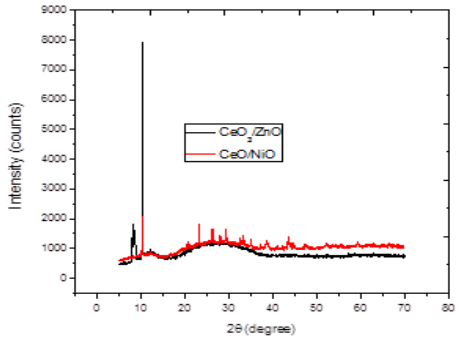

Fig. 3. XRD patterns of the films for as-deposited.

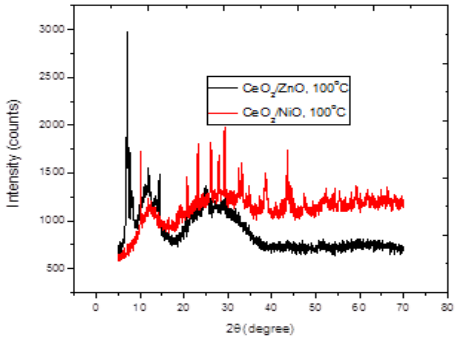

Fig. 4. XRD patterns of the films for annealed at 100°C.

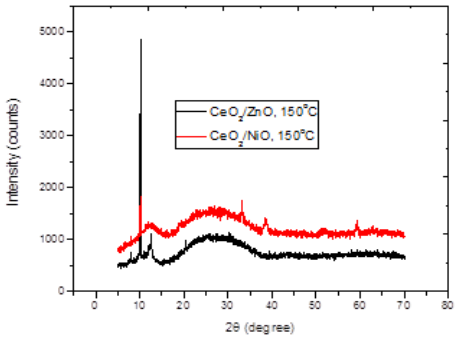

Fig. 5. XRD patterns of the films for annealed at 150°C.

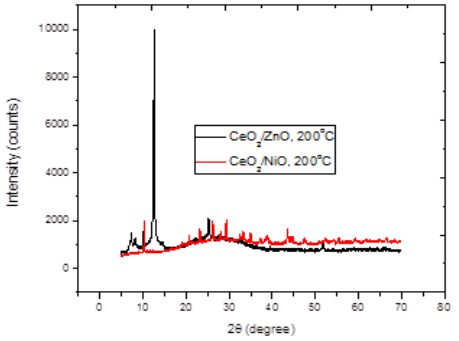

Fig. 6. XRD patterns of the films for annealed at 200°C.

3.3. Microstructural analysis

The microstructures of CeO_2/ZnO and CeO_2/NiO core-shell thin films are shown in figures 7 and 8 respectively. CeO_2/ZnO thin film exhibited more uniformity of particles aggregation and distribution compared to CeO_2/NiO core-shell thin film.

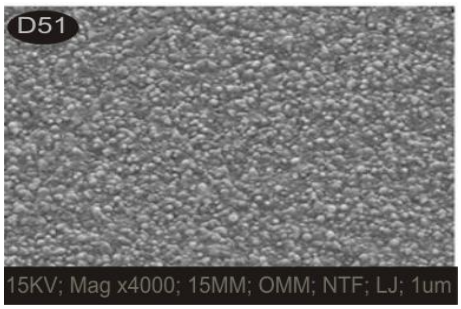

Fig. 7. Microstructure of CeO_2/ZnO core-shell thin film.

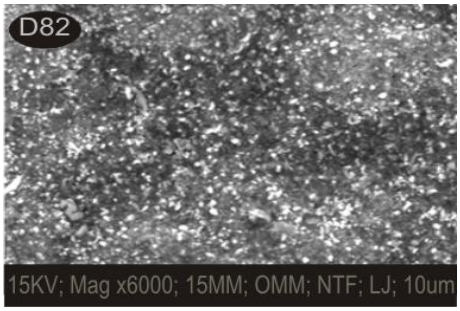

Fig. 8. Microstructure of CeO_2/NiO core-shell thin film.

3.4. Optical properties

Fig.9 depicts the plots of transmittance against wavelength while Figs. 10, 11 and 12 depict the plots of transmittance against wavelength for annealed at 100°C, 150°C and 200°C respectively.

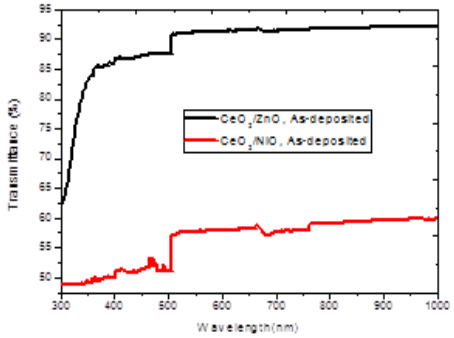

Fig. 9. Plots of T against λ for as-deposited.

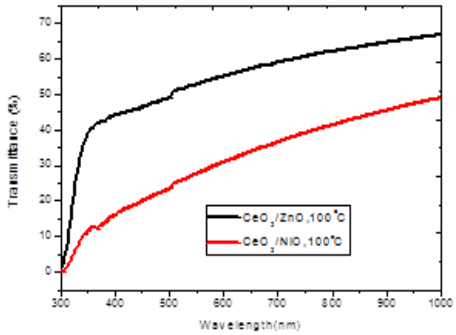

Fig. 10. Plots of T against λ for annealed at 100°C.

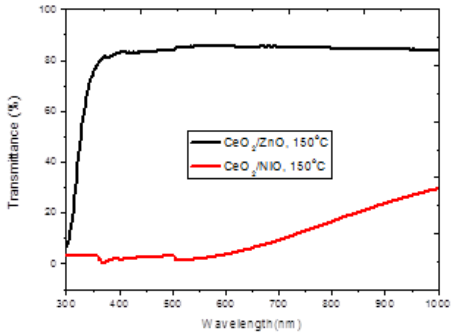

Fig. 11. Plots of T against λ for annealed at 150°C.

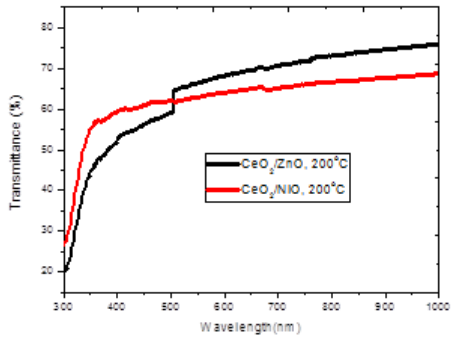

Fig. 12. Plots of T against λ for annealed at 200°C.

A steep fall in the fundamental edge independent of the annealing temperatures was observed in almost all the film samples. The plots (Fig.9-12), indicated a sharp rise in transmittance of CeO_2/ZnO layer relative to CeO_2/NiO layer near the band edge attributed to good crystallinity of the films [21]. The transmittance of CeO_2/ZnO layer is generally higher compared to CeO_2/NiO at each wavelength across the UV, Vis and infrared regions except in Fig.12, where CeO_2/NiO transmits higher in the wavelength range of 300-500nm. It is found that the transmittance of the films is enhanced in the visible near- IR region in the range from 500 to 1000 nm. Transmittance peaks of (92%, 55%), (65%, 45%), (83%, 30%) and (73%, 63%) were observed in figures 9, 10, 11 and 12 respectively for (CeO_2/ZnO, CeO_2/NiO). Ideally, the solar control coatings must enable controlled optical transmittance (T~10~50%) and low reflectance in the visible region (400-700nm) [22]. Such characteristics have been shown to provide an adequate natural illumination of the interior of the buildings, while rejecting as much of the incident radiation which might cause an undesirable increase in the interior temperature of the buildings

and thereby increase cooling costs in locations with warm climates. In view of these characteristics, CeO_2/ZnO and CeO_2/NiO core-shell thin films can efficiently be used in solar control coatings. Figures 13, 14, 15 and 16 are the plots of absorption coefficient as function of photon energy for as-deposited, annealed at 100°C, 150°C and 200°C respectively for CeO_2/ZnO and CeO_2/NiO core-shell thin films. The absorption coefficient of all films increased with increasing photon energy exhibiting a maximum in the infrared region. CeO_2/NiO film exhibited higher absorption coefficient compared to CeO_2/ZnO films as seen in fig. 13, 14 and 15 whereas fig.16 indicates that CeO_2/ZnO film absorb higher than CeO_2/NiO film.

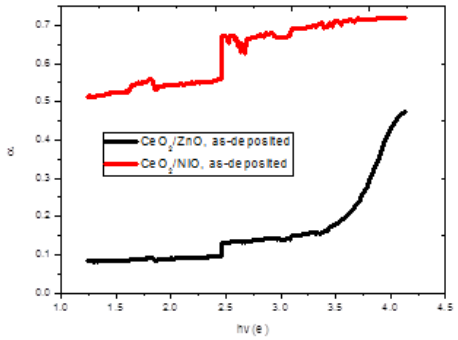

Fig. 13. Plots of α against hν for as-deposited.

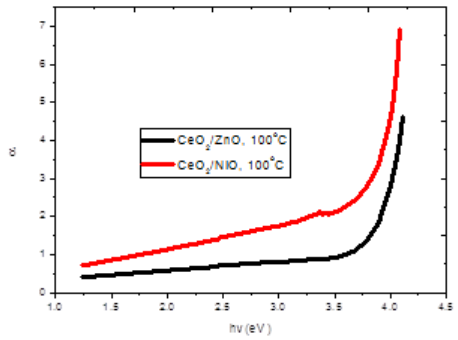

Fig. 14. Plots of α against hν for annealed at 100°C.

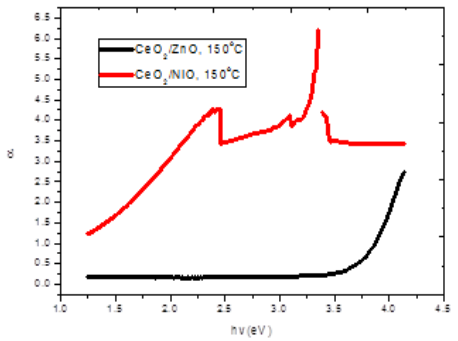

Fig. 15. Plots of α against hν for annealed at 150°C.

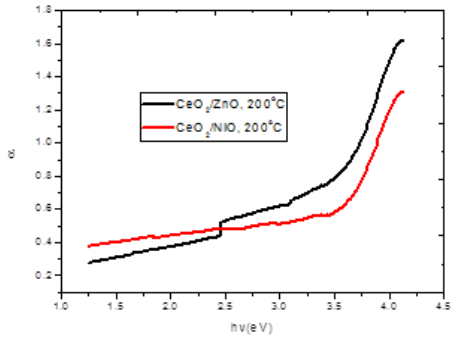

Fig. 16. Plots of α against hν for annealed at 200°C.

The absorption coefficient values were computed using mathematical relation available in the literature [23]. The high value of the optical absorption coefficient is an indication that the films can be utilized in different optoelectronic devices [24].

$$\alpha = \frac{1}{t}\ln\left(\frac{100}{T\%}\right) \tag{1}$$

where α is the absorption coefficient, t is thickness and T is the transmittance. The optical band gap (E_g) extracts from figures 17, 18, 19 and 20 respectively, in view of the changes in annealing temperature are shown on Table 1. The values obtained from these figures are in the range of 1.75eV-3.85eV for CeO_2/ZnO films and 3.50eV-3.88eV for CeO_2/NiO films. Some of these values are higher compared to the value (3.2eV) reported for CeO_2 thin film deposited by chemical bath deposition [25]. This is an indication that the shell impacted on the core by tailoring the band gap away from the fundamental absorption edge. It is seen that both core-shell thin films differed in their band gaps for as-deposited and annealed layers. As observed in fig.1-3, the band gap of CeO_2/ZnO films was lower compared to CeO_2/NiO films whereas in fig.4, CeO_2/ZnO film has a higher band gap than CeO_2/NiO thin films. These band gap tailoring from their binary origin offered them for special applications.

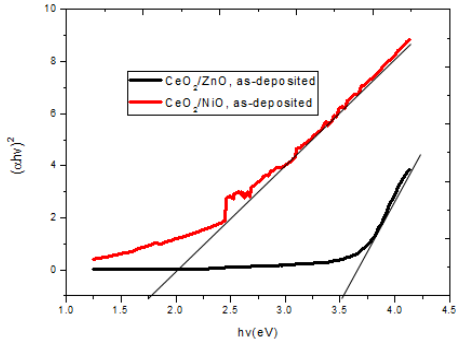

Fig. 17. Plots of $(\alpha h\nu)^2$ against hν for as-deposited.

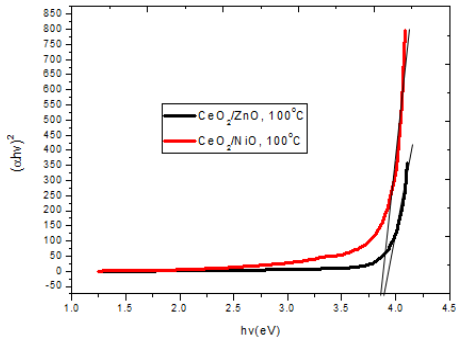

Fig. 18. Plots of $(\alpha hv)^2$ against hv for annealed at 100°C.

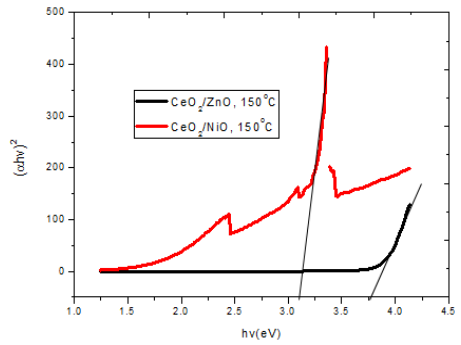

Fig. 19. Plots of $(\alpha hv)^2$ against hv at 150°C.

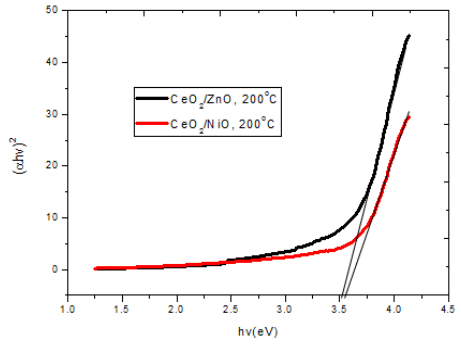

Fig. 20. Plots of $(\alpha hv)^2$ against hv for annealed at 200°C.

Table 1. Optical band gap values of film samples at different annealing temperature.

Sample	E_g (eV) before annealing	E_g (eV) after annealing at		
		100°C	150°C	200°C
CeO_2/ ZnO	1.75	3.85	3.15	3.60
CeO_2/ NiO	3.60	3.88	3.75	3.50

The direct band gap extracts above were determined from Tauc's relation from which the plots of $(\alpha hv)^2$ *vs* hv down the photon energy axis give the energy band gap.

$$(\alpha h\nu) = \mathrm{B}\left(h\nu - \mathrm{E}_g\right)^n \tag{2}$$

where in equation 2, α is the optical absorption coefficient, B is an energy independent constant but depend on the refractive index and the effective masses of the hole and electron respectively [26], E_g is the energy band gap, and n is an index that characterises the nature of the transition. For n = 1/2, the transition is generally accepted to be direct. According to the literature [27, 28], B is given by the equation;

$$B \approx \frac{q^2\left[2\dfrac{M_h^* M_e^*}{M_h^* + M_e^*}\right]^{\frac{3}{2}}}{nch^2 M_e^*} \tag{3}$$

where q is the electronic charge, n is the refractive index, c is the speed of light in free space, h is the Planck's constant, m_e and m_h are the effective masses of the electrons and holes respectively. According to Literature, wide band materials (WBG) have band gaps on the order of 2 to 4eV [29, 30]. They permits devices to operate at much higher voltages, frequencies and temperatures than convectional semiconductor materials. These properties make WBG materials useful in high power applications, light emitting diodes and transducers. The index of refraction, n is an important parameter for optical applications. Figures 21, 22, 23 and 24 show the plots of refractive index as a function of photon energy for as-deposited, annealed at 100^{o}C, 150^{o}C and 200^{o}C respectively. The complex optical refractive index is described according to the relation [31].

$$\bar{n} = n(w) + ik(w) \tag{4}$$

where n is the real part of and k is the imaginary part (extinction coefficient) of the complex refractive index. The refractive index of the film samples was computed using the relation [32].

$$n = \frac{1+R}{1-R} + \sqrt{\frac{4R}{\left(1+R^2\right)} - k^2} \tag{5}$$

where R is reflectance and k is the extinction coefficient. The result of Fig.13 shows an increasing trend of the refractive index with decreasing wavelength (increasing photon energies) for CeO_2/ZnO film samples whereas a rise and fall pattern was observed for CeO_2/NiO film samples. However, both films recorded an appreciable increase in refractive index between 3.25-4.25eV (Fig.21). CeO_2/NiO films generally exhibit higher refractive index compared to CeO_2/ZnO films. In all the figures, the average refractive index value was below 2. It has been reported that materials with average refractive index below 2 could be employed as anti-reflecting coating material and could improve the transmittance of glass from 0.9 to 0.96 [33]. In fig.22, both films exhibited similar refractive index values. In fig.23, the refractive index of CeO_2/ZnO film sample was fairly constant whereas that of CeO_2/NiO films fluctuates between negative minima and positive maxima. In Fig.24, both film samples exhibit similar patterns.

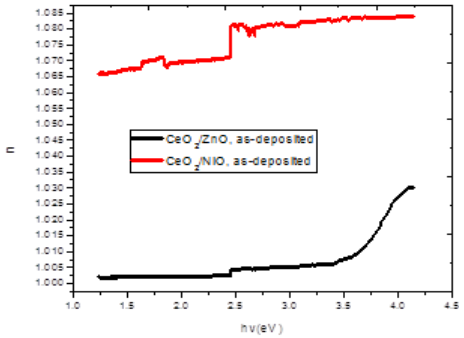

Fig. 21. Plots of n against hν for as-deposited.

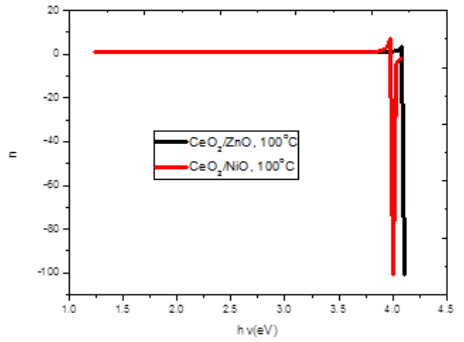

Fig. 22. Plots of n against hν for annealed at 100°C.

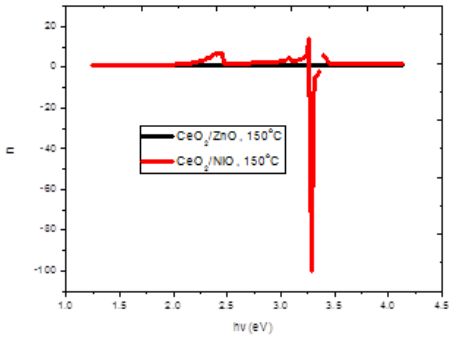

Fig. 23. Plots of n against hν for annealed at 150°C.

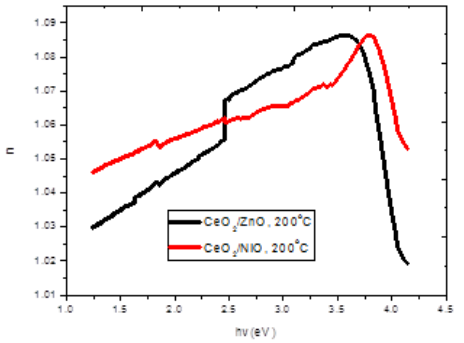

Fig. 24. Plots of n against hν for annealed at 200°C.

The extinction coefficient which is the sum of the absorption coefficient and scattering coefficient was computed and plotted against photon energy (hv) at different annealing temperature for both film samples. Such plots are shown in Fig. 25 to 28 for both the as-deposited and annealed layers. Fig.25 depicts extinction coefficient minima of 1.75 and maximum of 4.1 for CeO_2/NiO film sample whereas a minima and maxima of 0.7 and 1.15 respectively for CeO_2/ZnO film sample was observed. A sharp increase in extinction coefficient with increasing photon energy (decreasing wavelength) occurred between 3.50-4.20eV for both film samples as shown in Fig.26 with CeO_2/NiO layer exhibiting a maximum.

It is also evident from the plots (fig. 25) that the extinction coefficient decreased up to the range of the photon energies at which the energy band gaps occurred (region of the fundamental absorption) and then increased. Fig.27 indicates a decrease in extinction coefficient of CeO_2/ZnO layer between 1.25-3.5eV above which a steady increase occurred whereas CeO_2/NiO layer is characterized by rise and fall values of the extinction coefficient. In Fig.28, the extinction coefficients of CeO_2/ZnO and CeO_2/NiO films behave alike except that CeO_2/ZnO layer has minima and maxima of 2.2 and 3.90 respectively while the extinction coefficient minima and maximum for CeO_2/NiO layer are 3.0 and 3.20 respectively. The values of the extinction coefficient was generated using the relation [34].

$$k = \frac{\alpha\lambda}{4\pi} \tag{6}$$

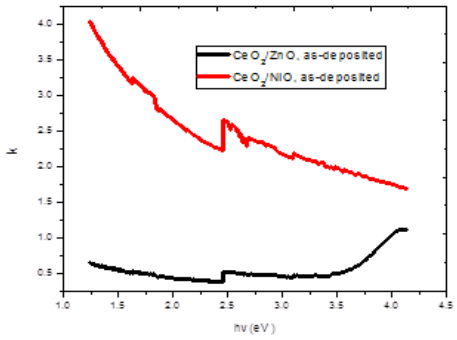

Fig. 25. Plots of k against hv for as-deposited.

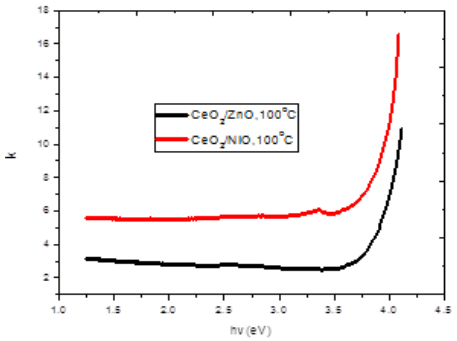

Fig. 26. Plots of k against hv for annealed at 100°C.

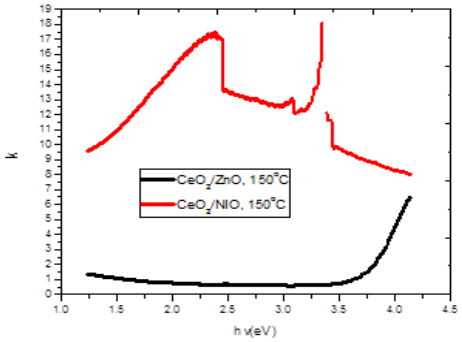

Fig. 27. Plots of k against hν for annealed at 150°C.

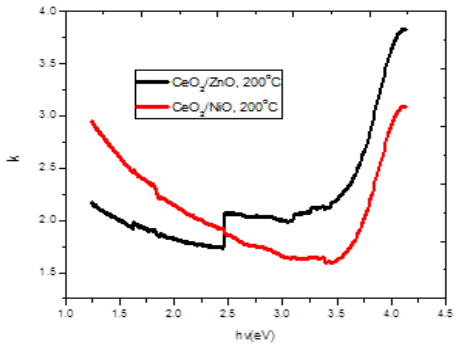

Fig. 28. Plots of k against hν for annealed at 200°C.

The complex dielectric constant is a fundamental intrinsic property of the material. The real part of the dielectric constant shows how much the speed of light slows down in the material, whereas the imaginary part shows how a dielectric material absorbs energy from an electric field due to dipole motion. Figures 29, 30, 31 and 32 depict the plots of imaginary dielectric constant against photon energy for as-deposited, annealed at 100°C, 150°C and 200°C respectively for both film samples. The values were generated using equation 9 and plotted against photon energy (Fig.29-32). The dielectric constant is a complex quantity that is related to the complex refractive index by the mathematical relation [34].

$$\varepsilon = \varepsilon_r + \varepsilon_i = (n - ik)^2 \tag{7}$$

where ε_r and ε_i are the real and imaginary parts respectively of dielectric and $(n - ik)$ is the complex refractive index. Hence,

$$\varepsilon_r = n^2 - k^2 \tag{8}$$

$$\varepsilon_i = 2ink \tag{9}$$

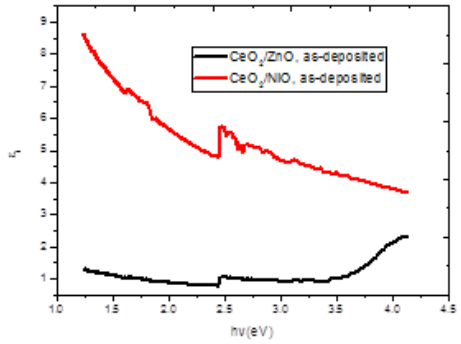

Fig. 29. Plots of ε_i against hν for as-deposited.

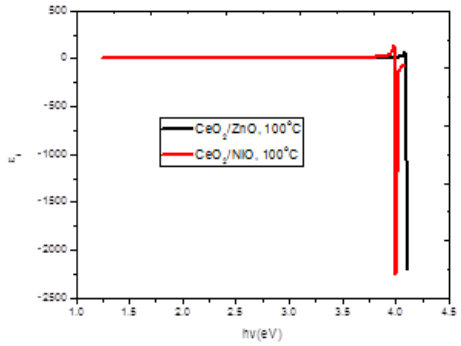

Fig. 30. Plots of ε_i against hν for annealed at 100^{o}C.

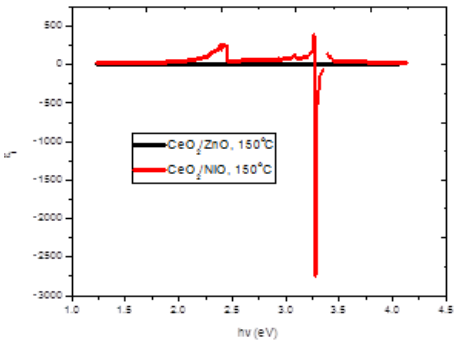

Fig. 31. Plots of ε_i against hν for annealed at 150^{o}C.

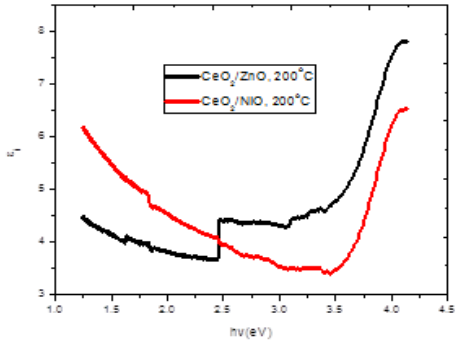

Fig. 32. Plots of ε_i against hν for annealed at 200^{o}C.

It is observed from the plots of imaginary dielectric constant against photon energy that CeO_2/ZnO layer generally has higher values compared to CeO_2/NiO layer with the exception of Fig.32, where the reverse is the case.

4. Conclusions

The comparative study of CeO_2/ZnO and CeO_2/NiO core-shell thin films grown using chemical bath deposition technique have been analysed, with emphasis on the effect of annealing temperature on the optical band gap. The results of the investigations shows that the band gap of the deposited thin films were direct and ranges from 1.75 eV to 3.85 eV for CeO_2/ZnO film samples and 3.50 to 3.88eV for CeO_2/NiO film samples. The band gaps are in the range suitable for use in various solar architecture.

References

[1] Z. Rehana, Ph.D Thesis, Department of Physics, Lahore College for Women University, Lahore, Pakistan.
[2] T. Minami, Semiconductor Science and Technology **20**(4), 535 (2005).
[3] A. Yoshikawa, Development and applications of wide band gap semiconductors, wide band gap semiconductors, springer, **2** (2007).
[4] S. Shyh-Chiang, Wide-bandgap device research and development, Georgia institute of Technology semiconductors research laboratory, (2014).
[5] C. Mansilla, Solid State Sciences **11**(8), 1456 (2009).
[6] G. Balakrishnan, P. Kuppusami, T. N. Sairam, R. Tirumurugesan, E. Mohandas, D. Sastikumar Journal of Nanoscience and Nanotechnology **9**(9), 5421 (2009).
[7] A. E. Ajuba, S. C. Ezugwu, P. U. Asogwu, F. I. Ezema, Chalcogenide Letter **10**, 573 (2010).
[8] M. Saleem, L. Fang, H.B. Ruan, F. Wu, Q.L. Huang, C.L. Xu, C.Y. Kong, International Journal of Physical Sciences **7**(23), 2971 (2012).
[9] H. Chen, Y. Lu, W. Hwang, Surface and Coating Technology **198**, 138 (2005).
[10] A. E. Ajuba, S. C. Ezeugwu, P. U. Asogwa, F. I. Ezema, Chalcogenide Letter **10**(7), 573 (2010).
[11] A. Fuchs, M. Bogner, K. Shangal, R. Winter, T. Dell, I. Eisele, Sens. Actuators B. Chem. **47**, 145 (1998).
[12] T. Miki, K. Yoshimura, S. Tanemura, Jpn. J. Appl. Phys. **34**, 240 (1995).
[13] A. Tomozawa, F. Fujii, H. Torii, R. Takayama, Jpn. J. Appl. Phys. **35**, 1328 (1996).
[14] T. Minami, H. Sati, S. Takata, T. Y. Yamada, Thin Solid Films **27**, (1995).
[15] D. U. Onah, D. E. I. Ugwu, J. E. Ekpe, American Journal of Nano Research and Applications **3**(3), 62 (2015).
[16] C. Augustine, M. N. Nnabuchi, F. N. C. Anyaegbunam, A. N. Nwachukwu, Digest Journal of Nanomaterials and Biostructures **12**(2), 523 (2017).
[17] C. Augustine, M. N. Nnabuchi, Materials Research Express **5**(2), 1 (2018).
[18] M. N. Nnabuchi, C. Augustine, Materials Research Express **5**(3), 1 (2018).
[19] C. Augustine, M. N. Nnabuchi, F. N. C Anyaegbunam, C. U. Uwa, Chalcogenide Letters **14**(8), 321 (2017).
[20] C. Augustine, M. N. Nnabuchi, Journal of Ovonic Research **13**(4), 233 (2017).
[21] M. A. Al-Sabayleh, J. Sci. Med. Eng. **20**, 17 (2008).
[22] P. K. Nair, M. T. S. Nair, Solar Energy Materials **15**, 431.
[23] P. E. Agbo, P. A. Nwofe, L. O. Odo, Chalcogenide Letters **14** (8), 357 (2017).
[24] P. A. Nwofe, P. E. Agbo, Journal of Non-Oxide Glasses **9**(1), 9 (2017).
[25] C. Mansilla, Solid State Sciences **11**(8), 1456 (2009).
[26] J. Bardeen, F. J. Blatt, L. H. Hall, (1954), Proc. of Atlantic City Photoconductivity Conference, J. Wiley and Chapman and Hall (1956).

[27] J. I. Pankove, Optical Processes in Semiconductors, Prentice-Hall, Englewood Cliffs, New Jersey, 1971.
[28] P. A. Nwofe, P. E. Agbo, Journal of non-oxide glasses **9**(1), 9 (2017).
[29] A. Yoshikawa, Development and applications of wide band gap semiconductors, wide band gap semiconductors, springer, 2 (2007).
[30] Shen Shyh-Chiang, Wide-bandgap device research and development, Georgia institute of Technology semiconductors research laboratory (2014).
[31] K. Kamiya, J. Cookson, Plantinum Metals Rev. **56**, 83 (2014).
[32] J. S. Cruz, D. S. Cruz, M. C. Arenas-Arrocena, F. D. M. Flores, S. A. M. Hernandez, Chalcogenide Letters **12**(5), 277 (2015).
[33] Chikwenze, R. A., Ph.D Thesis, Department of Industrial Physics, Ebonyi State University, Abakaliki, 2011.
[34] B. G. Mahrov, A. Hgfeldt, L. Dloczuk, T. Dittrich, Appl. Phys. Lett. **84**(26), 5455 (2004).